grains, and $E_c^0 >> kT$. As $x \rightarrow 3$, these assumptions fail as the arguments of the exponentials approach zero. We cannot say how tightly coupled the grains become in the real system; it is possible that disorder on the grain boundaries may not allow the metallic regions to completely merge.

We have made an ad hoc improvement to the theory that has the proper behavior as $E_c^0 \rightarrow 0$ and can represent granular metal conductivities and percolation well:

$$\rho = \frac{2h}{e^2}\frac{(d+s)}{\gamma}\sinh\left(\frac{E_c^0}{2kT}\right)\exp(2\chi s) + \rho_g \tag{3}$$

where $\rho_g$ is a resistivity contribution from intragrain scattering. Our motivation for the replacement exp() → 2sinh() is that, as $E_c^0 \rightarrow 0$, the barriers to conduction vanish and $\rho \rightarrow 0$ (neglecting intragrain scattering). Fits with this modified theory are similar, with $L = 75$ Å, $\gamma = 6$, $\chi = 0$, and $\rho_g = \rho(x = 3)$. The data cannot be fit well using any reasonable effective medium model unless the conductivity of the percolating phase has a similar activated behavior.

The fitted values of $L$ are in good agreement with the 60 Å grain size for the $C_{60}$ film before doping. The result $\chi = 0$ implies that the energy barriers between grains are comparable to the charging energies (*17*), and about as many electrons go over the barriers as go through them. The fitted values of $\gamma$ are close enough to unity to be plausible in the absence of a complete theory (*18*).

Stoichiometries of films of various thicknesses are shown in Fig. 4. The filled symbols correspond to doping at either the $R_{\min}$ or $R_{\max}$ points in plots of resistance versus K exposure. These points fall to within an error of ±0.05 on solid lines drawn respectively for the precise stoichiometries at $x = 3$ or $x = 6$. Although implied by existing work (*1*), this result demonstrates that the conductivity extrema fall exactly at half and full band filling.

In summary, the diffusion of K into $C_{60}$ films produces a minimum resistivity phase that is barely metallic with $\rho = 2.2$ microohm-cm at composition $K_{3.00\pm0.05}C_{60}$, and a high resistivity (max) phase at composition $K_{6.00\pm0.05}C_{60}$. Intermediate compositions yield activated conduction with $x$-dependent activation energy, which can be explained by a simple model with immiscible phases where the metallic phase maximally avoids percolation. The recognition that the normal state has a granular microstructure will also be important in understanding superconductivity in thin films.

### REFERENCES AND NOTES

1. R. C. Haddon *et al.*, *Nature* **350**, 320 (1991).
2. A. F. Hebard *et al.*, *ibid.*, p. 600.
3. R. M. Fleming *et al.*, *Mater. Res. Soc. Symp. Proc.* 206, 691 (1991).
4. P. W. Stephens *et al.*, *Nature* **351**, 632 (1991).
5. R. M. Fleming *et al.*, *ibid.* **352**, 701 (1991).
6. O. Zhou *et al.*, *ibid.* **351**, 462 (1991).
7. R. Tycko *et al.*, *Science* **253**, 884 (1991).
8. D. M. Poirier *et al.*, *ibid.*, p. 646.
9. C. T. Chen *et al.*, *Nature* **352**, 603 (1991).
10. K. Holczer *et al.*, *Science* **252**, 1154 (1991).
11. W. Krätschmer, L. D. Lamb, K. Fostiropoulos, D. R. Huffman, *Nature* **347**, 354 (1990).
12. A. F. Hebard, R. C. Haddon, R. M. Fleming, A. R. Kortan, *Appl. Phys. Lett.* **59**, 2109 (1991).
13. B. Abeles, P. Sheng, M. D. Coutts, Y. Arie, *Adv. Phys.* **24**, 407 (1975).
14. The temperature coefficient of resistance, $R^{-1}dR/dT$ is negative for all films, except for $2.8 < x < 3.2$ where the behavior is metallic with $R^{-1}dR/dT = (7.9 \pm 0.4) \times 10^{-4}\ K^{-1}$ at $x = 3$. The width of the resistance minimum (and the region of positive temperature coefficient) is comparable to our estimates of doping uniformity (10%), so an ideal experiment might reveal a sharp minimum.
15. B. Abeles, *Appl. Solid State Sci.* **6**, 1 (1976).
16. If the grains were spheres on a simple cubic lattice, they would intersect at $x = \pi/6$; the intersection would correspond to a percolation threshold. Because we see no percolation until $x \approx 3$, the expression we use (corresponding to a lattice of cubes) is the simplest choice.
17. In the derivations in (*15*), the assumption is made that the barrier is large compared to the charging energies. What is referred to as the "barrier height" is more accurately the barrier height above the charging energy.
18. The calculation of $\gamma$ in (*15*) is only valid in the limit $\chi(d + s) >> 1$; its derivation assumes the strong dependence of current on grain separation that is characteristic of a tunneling process.
19. We thank E. E. Chaban, D. J. Eaglesham, R. H. Eick, R. M. Fleming, A. R. Kortan, A. V. Makhija, D. W. Murphy, T. T. M. Palstra, J. C. Phillips, M. J. Rosseinsky, J. E. Rowe, F. C. Unterwald, B. E. Weir, and G. K. Wertheim for their contributions to this work.

19 September 1991; accepted 7 November 1991

---

# Hydrogen as a Probe of Semiconductor Surface Structure: The Ge(111)-c(2 × 8) Surface

JOHN J. BOLAND

**Hydrogen can be used as an effective probe of the structure of semiconductor surfaces. Such surfaces consist of bonds with varying degrees of bond strain, and hydrogen can react with each selectively depending on the reaction conditions. This selectivity is derived from a reduced barrier to reaction associated with strained bonds. In this manner, hydrogen can be used to pick apart the surface one bond type at a time, thereby revealing the structure of even complex multilayer reconstructions. This method is used to directly show that the rest-layer of the Ge(111)-c(2 × 8) surface has a bulk structure.**

THE CHEMISTRY OF SEMICONDUCTOR surfaces is of great technological importance and an understanding of this chemistry requires a detailed knowledge of the surface structure. The surfaces of semiconductors typically reconstruct and form structures that differ substantially from those of the bulk (*1*). Surface reconstructions are often complex and may extend for several layers beneath the surface. This is particularly true of (111) surfaces; (100) surfaces, however, usually form simple single-layer dimer reconstructions. The structure of such complex multilayer reconstructions cannot be resolved by conventional surface scattering techniques. However, the advent of scanning tunneling microscopy (STM) offers the unprecedented capability to study surfaces at the atomic level (*2*). Although this technique can be used to determine the structure of the outermost surface layer, the structure of the underlying layers cannot be readily studied. This report describes the use of atomic hydrogen as an effective means of exposing and stabilizing these underlying layers. Once exposed, these layers may be directly probed by STM. This technique has been used to study the structure of the Ge(111)-c(2 × 8) surface and to show directly that it is a pure adatom surface, the underlying layer having a bulk (1 × 1) structure.

The Ge(111) surface consists of an outer layer of Ge adatoms that are arranged in a c(2 × 8) structure (*3*). Each adatom has three backbonds to the layer beneath, the so-called rest-layer. The remaining bonding orbital constitutes the unsaturated adatom dangling bond. The structure of this rest-layer has not been definitively established. Early STM studies of this surface clearly showed the c(2 × 8) adatom structure (*3*). However, the structure of the rest-layer had to be inferred from regions of this layer that were imaged between the gaps in the structure of the outer adatom layer. Based on this analysis, the rest-layer was suggested to have a bulk structure (*3*). This structure is consistent with the presence of bilayer-deep holes that form after the (2 × 1) to c(2 × 8) transformation on the Ge(111) surface (*4*). However, a more recent STM study has shown that there exists an asymmetry in the

IBM Research Division, Thomas J. Watson Research Center, Yorktown Heights, NY 10598.

c(2 × 8) unit cell similar to that previously reported on the Si(111)-(7 × 7) surface (*5*). The rest-layer in the latter case is known to have a nonbulk structure (*6*). Furthermore, a recent lattice-gas model of the Ge(111) surface suggests a dimer instead of a simple adatom structure (*7*). Here, hydrogen chemistry and the structural properties of the Ge surface are used to directly determine the structure of this rest-layer.

The STM used in this experiment is similar to that described by Demuth *et al.* (*8*) and was mounted in a vacuum chamber with a base pressure of less than $8 \times 10^{-11}$ torr. The sample was a 0.4 Ω-cm Sb-doped Ge(111) wafer that was annealed at 1120 K for 10 min and cooled slowly (~2 K per second) to prepare the c(2 × 8) surface. The tip preparation and method of hydrogen exposure have been described in detail elsewhere (*9*).

The STM image in Fig. 1A shows that the Ge(111) surface largely consists of a c(2 × 8) adatom structure. The average size of the c(2 × 8) domains is small (~200 Å), in agreement with earlier studies (*3*). Several rotationally equivalent domains are typically observed on a given terrace, and the boundaries between these domains are accommodated by the formation of local (2 × 2) adatom structures. One such boundary region is shown in the lower section of Fig. 1A. The surface following a saturation exposure to atomic hydrogen is shown in Fig. 1B. For comparison purposes the areas shown in Fig. 1, A and B, are the same size. However, the black-to-white gray-scale range is three times larger in Fig. 1B. The adatoms that originally comprised the outer surface layer shown in Fig. 1A have clustered together to form adatom islands in Fig. 1B. The rest-layer, to which the adatoms were originally bound, is now exposed and exhibits a densely packed bulk (1 × 1) structure.

The ability of hydrogen to uncover the detailed structure of semiconductor surfaces is derived from the nature of the bonding in these materials. The atoms within bulk Ge or Si are bound together by directional covalent bonds. The surfaces of such materials reconstruct to reduce the number of dangling bonds, thereby minimizing the surface free energy. In doing so the surface atoms are forced to adopt a bonding configuration that may differ substantially from that of the bulk. Covalently bonded materials are very sensitive to bond deformations, and the surface bonds may be highly strained as a result. Thus a strain field exists on the surface of semiconductor materials that extends from the surface into the bulk. The magnitude and extent of this strain field depends on the nature of the surface reconstruction. In all cases the strain field is reduced to zero when the bulk structure is reestablished at some distance beneath the surface.

It is the presence of these strained surface bonds that allows hydrogen to probe the structure of semiconductor surfaces. Strained bonds, by their very nature, are weaker than those bonds that make up the bulk and are more susceptible to reaction. This behavior is shown schematically in Fig. 2, which shows the potential energy of reaction for various surface bonds. The reaction of hydrogen atoms with any Ge–Ge bond (or Si–Si bond, for that matter) is thermodynamically favorable. However, the rate of reaction depends upon the nature of the bond. Strain weakens bonds and enhances their reactivity, which manifests itself as a reduced barrier to reaction (Fig. 2). If the transition state is assumed not to be strain-dependent, then the enhanced reactivity of strained bonds is simply given by:

$$k_s/k_b \approx \exp(\Delta E/kT) \qquad (1)$$

where $\Delta E$ is the strain energy, $k_s$ and $k_b$ are the rates of reaction for strained and bulk bonds, respectively, $k$ is the Boltzmann's constant, and $T$ is the absolute temperature. This enhancement can be very significant. For instance, in the case of the Si(111)-(7 × 7) surface the backbond strain energy is estimated (*10*) to be ~1.1 eV, so that $k_s/k_b \approx 10^{18}$ at room temperature. Therefore, if a surface presents a variety of different bonds to the incoming hydrogen atoms, the most highly strained bonds react first. Hydrogen then reacts successively with the remaining surface bonds, the order of which is determined by strain energy. Reaction with bulk bonds occurs only following reaction of all of the strained surface bonds. Thus the strain field insures that the reaction proceeds from the outermost surface layer downwards toward the bulk and exposes the nature of the surface structure as the reaction proceeds. In practice, the various surface bonds may have very different strain energies, which require changes in the reaction conditions to enable the reaction to proceed from one bond type to the next. This procedure allows the surface structure to be studied by STM following each stage of the reaction, thereby providing

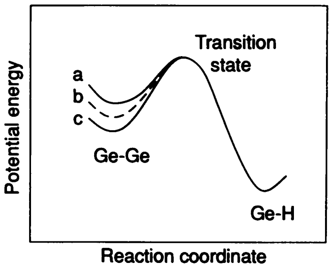

**Fig. 2.** Schematic of the potential energy versus reaction coordinate for the reaction of different surface bonds with atomic hydrogen: (a) a highly strained backbond; (b) (dashed curve) a bond of intermediate strain, such as a dimer bond on the Si(111)-(7 × 7) surface; and (c) a relaxed bulk bond of the Ge(111) surface. Note that bond strain reduces the barrier to reaction.

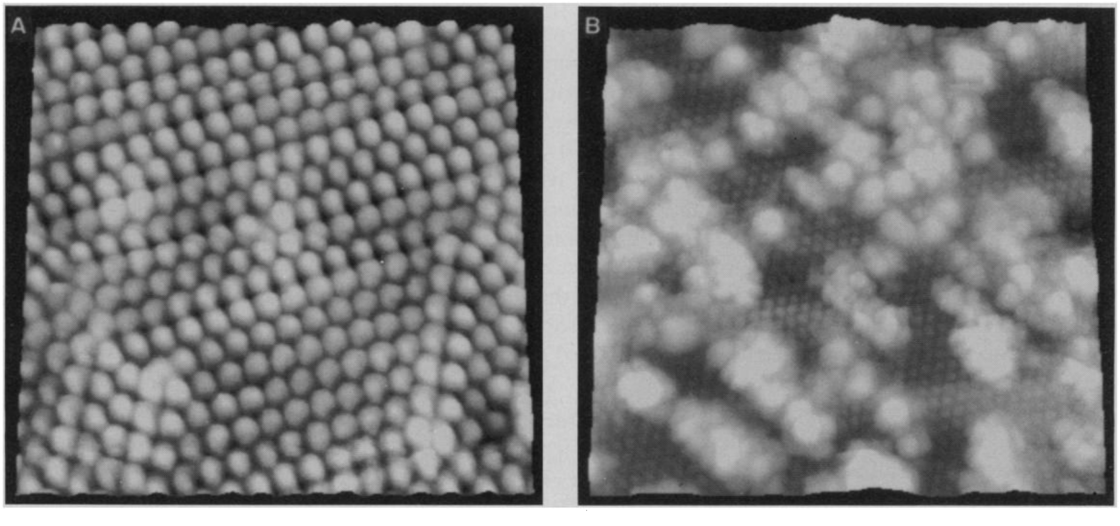

**Fig. 1.** (**A**) The original Ge(111)-c(2 × 8) surface. The area shown is 145 Å by 145 Å and was recorded at a sample bias of +1.5 V. Gray-scale range is 2 Å. Note domain boundary in lower section of image. (**B**) A Ge(111) surface following a saturation exposure to atomic hydrogen and a brief 365 K anneal. The area shown is 145 Å by 145 Å and was recorded at a bias of +1.5 V. Gray-scale range is 6 Å. Note the bulk (1 × 1) rest-layer structure. Shadows are an artifact of the background substraction.

a picture of the bonding at different levels in the reconstruction.

On the basis of the data in Fig. 1B, the Ge(111) surface consists of an outer adatom layer and a rest-layer that has a bulk (1 × 1) structure. The backbonds that bind these adatoms to the rest-layer are known to be highly strained (*11*). After reaction with the dangling surface bonds, hydrogen proceeds to attack these strained backbonds, which results in bond scission. Hydrogen reacts with the dangling bonds generated by this bond scission, thus stabilizing the (1 × 1) bulk rest-layer structure and hydrogenating the adatom species. Further reaction with this adatom species results in further backbond scission and hydrogenation, and ultimately $GeH_4$ formation. In this manner, the adatoms are removed and the underlying rest-layer is exposed. However, not all of the adatoms react in this manner. Hydrogen also facilitates the formation of hydrogenated adatom islands on the surface. This is an alternative mechanism to relieve the strain in the backbonds and results in the formation of islands with largely relaxed Ge–Ge bonds. Similar mechanisms were observed on the Si(111)-(7 × 7) surface (*9, 12, 13*). In each case, these reactions serve to expose the underlying rest-layer and allow it to be directly imaged by the STM. On the other hand, reaction of the unstrained rest-layer bonds is very slow and is not observed under the present conditions. In addition to the larger barrier associated with this reaction, the compact (111) structure limits the ability of hydrogen to penetrate the surface (*14*).

This technique is not limited to Ge surfaces; the structure of the Si(111)-(7 × 7) surface can be probed in a similar manner (*9, 12, 13*). The Si(111) surface also has an adatom surface layer but the rest-layer beneath has a nonbulk structure consisting of triangular subunits bounded by rows of dimers (*6*). As in the case of the Ge(111) surface, reaction at room temperature exposes the rest-layer through $SiH_4$ and adatom island formation. The moderately strained dimer bonds do not react under these conditions. However, by annealing or dosing at 550 K the dimer bonds gradually react and the rest-layer slowly adopts a bulk-like structure. The elevated reaction temperature is a reflection of the moderate strain associated with these dimer bonds and a correspondingly larger barrier to reaction (see Fig. 2). Here too the reactivity is controlled by bond strain, allowing hydrogen to sequentially react with, and effectively titrate, the different surface bonds.

Although the presence of this strain field is an intrinsic property of covalent semiconductor materials, not all adsorbates serve as useful probes of surface structure. The ideal adsorbate must be monovalent and form strong bonds with semiconductors so that the adsorbate can saturate the dangling bonds produced by bond scission and stabilize the exposed surface. The adsorbate should be small to avoid interadsorbate interactions and to penetrate the surface structure. Most importantly, however, the adsorbate must show selectivity between bonds with different degrees of strain. It is this characteristic that allows hydrogen to pick apart the reconstruction. Chlorine fails in this regard; both the backbond and dimer-bond reactions on the Si(111) surface proceed effectively only at elevated temperatures (*15, 16*). Bromine, however, is too large, and fluorine reactions are so exothermic that little selectivity is expected. This selectivity, together with the ability to react with and stabilize the dangling bonds of the exposed layer, makes hydrogen an effective chemical probe of surface structure.

REFERENCES AND NOTES

1. D. Haneman, *Rep. Prog. Phys.* **50**, 1045 (1987).
2. G. Binnig and H. Rohrer, *Helv. Phys. Acta.* **55**, 726 (1982).
3. R. S. Becker, B. S. Swartzentruber, J. S. Vickers, T. Klitsner, *Phys. Rev. B* **39**, 1633 (1989).
4. R. M. Feenstra and A. J. Slavin, *Surf. Sci.* **251/252**, 401 (1991).
5. E. S. Hirschorn, D. S. Lin, F. M. Leibsle, A. Samsavar, T.-C. Chiang, *Phys. Rev. B* **44**, 1403 (1991).
6. K. Takayanagi, Y. Tanishiro, M. Takahashi, S. Takahashi, *J. Vac. Sci. Technol. A* **3**, 1502 (1985).
7. Y. G. Hao and L. M. Roth, *Surf. Sci.* **232**, L201 (1990).
8. J. E. Demuth, R. J. Hamers, R. M. Tromp, M. E. Welland, *J. Vac. Sci. Technol. A* **4**, 1320 (1986).
9. J. J. Boland, *Surf. Sci.* **244**, 1 (1991).
10. I. Ohdamari, *ibid.* **227**, L129 (1990).
11. R. D. Meade and D. Vanderbilt, *Phys. Rev. B* **40**, 3905 (1989).
12. J. J. Boland, *J. Phys. Chem.* **95**, 1521 (1991).
13. ———, *J. Vac. Sci. Technol. B* **9**, 764 (1991).
14. ———, *Surf. Sci.* **261**, 17 (1992).
15. J. S. Villarrubia and J. J. Boland, *Phys. Rev. Lett.* **63**, 306 (1989).
16. J. J. Boland and J. S. Villarrubia, *Phys. Rev. B* **41**, 9865 (1990).

1 October 1991; accepted 31 October 1991

# Late Holocene Tectonics and Paleoseismicity, Southern Cascadia Subduction Zone

SAMUEL H. CLARKE, JR., AND GARY A. CARVER

**Holocene deformation indicative of large subduction-zone earthquakes has occurred on two large thrust fault systems in the Humboldt Bay region of northern California. Displaced stratigraphic markers record three offsets of 5 to 7 meters each on the Little Salmon fault during the past 1700 years. Smaller and less frequent Holocene displacements have occurred in the Mad River fault zone. Elsewhere, as many as five episodes of sudden subsidence of marsh peats and fossil forests and uplift of marine terraces are recorded. Carbon-14 dates suggest that the faulting, subsidence, and uplift events were synchronous. Relations between magnitude and various fault-offset parameters indicate that earthquakes accompanying displacements on the Little Salmon fault had magnitudes of at least 7.6 to 7.8. More likely this faulting accompanied rupture of the boundary between the Gorda and North American plates, and magnitudes were about 8.4 or greater.**

THE POTENTIAL FOR LARGE EARTHquakes along the Cascadia subduction zone (CSZ) has been controversial; some (*1*) have interpreted crustal deformation data and the absence of large magnitude thrust earthquakes during the last 150 years to indicate that plate convergence averaging 30 to 40 mm/yr (*2*) is accommodated by aseismic slip. Others (*2*) have noted that the lack of large magnitude subduction-related earthquakes, the young age of the subducted plate, the shallow dip of the subduction zone (10° to 15°), and the subdued offshore trench are consistent with strong coupling between the plates, and suggest that the CSZ is capable of producing great magnitude [$M_w > 8.5$; (*3*)] earthquakes.

The southern Cascadia subduction zone (SCSZ) and overlying accretionary prism lie partly offshore, but also extend onland in northern California (Fig. 1) (*4, 5*). As a result examination of the offshore structure of the subduction margin by acoustic-reflection techniques (*4, 6*) can be integrated with paleoseismic studies on land. In this report, we use dated fault displacements together with evidence of coincident coseismic uplift and subsidence to evaluate the Holocene seismic activity and earthquake potential of the SCSZ.

The accretionary prism of the SCSZ is 85 to 100 km wide and comprises prominent systems of north-northwest trending, east-

---

S. H. Clarke, Jr., Branch of Pacific Marine Geology, U.S. Geological Survey, 345 Middlefield Road, Mail Stop 999, Menlo Park, CA 94025.
G. A. Carver, Department of Geology, Humboldt State University, Arcata, CA 95521.